

Towards More Precise Photometric Redshifts: Calibration Via CCD Photometry

Robert J. Brunner^{1,2}, Andrew J. Connolly¹, and Alexander S. Szalay¹

rbrunner@pha.jhu.edu, ajc@pha.jhu.edu, szalay@pha.jhu.edu

Department of Physics & Astronomy, The Johns Hopkins University, Baltimore, MD 21218

and

Matthew A. Bershadsky¹

mab@astro.psu.edu

Department of Astronomy & Astrophysics, Penn State University, University Park, PA

16802

Received _____; accepted _____

¹Visiting Astronomer, Kitt Peak National Observatory, National Optical Astronomy Observatories, which is operated by the Association of Universities for Research in Astronomy, Inc. (AURA) under cooperative agreement with the National Science Foundation.

²NASA GSRP Fellow

ABSTRACT

We present the initial results from a deep, multi-band photometric survey of selected high Galactic latitude redshift fields. Previous work using the photographic data of Koo and Kron demonstrated that the distribution of galaxies in the multi-dimensional flux space $U, B, R, \& I$ is nearly planar. The position of a galaxy within this plane is determined by its redshift, luminosity and spectral type (Connolly *et al.* 1995). Using recently acquired deep CCD photometry in existing, published redshift fields, we have redetermined the distribution of galaxies in this four-dimensional magnitude space. Furthermore, from our CCD photometry and the published redshifts, we have quantified the photometric-redshift relation within the standard AB magnitude system. This empirical relation has a measured dispersion of $\sigma_z \approx 0.02$ for $z < 0.4$. With this work we are reaching the asymptotic intrinsic dispersions ($\sigma_z \approx 0.016$ for $z < 0.4$) that were predicted from simulated distributions of galaxy colors. This result will prove useful in providing estimated redshifts for large photometric surveys, as well as improve the sampling of specific redshift regions for spectroscopic surveys through the use of an estimated redshift selection criteria.

Subject headings: cosmology: observations - galaxies: evolution - galaxies: photometry

1. Introduction

The utility of deriving galaxy redshifts from photometric data has long been known (Baum 1962, Koo 1985, Loh & Spillar 1986). Recently, Connolly *et al.* 1995 developed an empirical approach as opposed to the previous model fitting methods. Utilizing photographic data, they were able to estimate a redshift out to $z \sim 0.5$ with a measured dispersion of $\delta z < 0.05$. The uncertainties in that result were dominated by the photometric errors. Simulations indicated that with improved photometry the dispersion within the relationship could be significantly reduced. As a result, we have embarked on an observational program designed to obtain deep CCD multi-band photometry in existing redshift fields.

In this paper we present the first results of this survey by extending the previous approach using CCD photometry. Section two outlines the basic reduction steps taken in the preparation of the sample for this work. Section three discusses the actual fitting techniques and investigates the intrinsic dispersion. We conclude this letter with a discussion of the ramifications of this work and possible future directions.

2. Data

The photometric data used in this analysis were taken using the PFCCD camera with the standard $U, B, R,$ & I filters on the Mayall 4m at Kitt Peak National Observatory on the nights of March 31 – April 3, 1995, March 18–20, 1996, and May 14–16, 1996. This camera uses a 2048^2 CCD ($T2KB$) with a $0.47''/\text{pixel}$ scale and a read noise of $4e^-/\text{pixel}$. The gain used for these observations was $5.4 e^-/ADU$, a value which resulted from a tradeoff between maximizing the available dynamic range and minimizing the effects of the charge depletion problem with the CCD electronics. These observations were chosen to

coincide with the published 14 hour redshift field of the Canada-France Redshift Survey (CFRS). A complete discussion of the observational program including an analysis of the custom reduction software are beyond the scope of this letter and will be published elsewhere (Brunner 1997).

All three runs were reduced separately using the standard IRAF routines. The images were initially debiased and flat fielded using dome flats. Illumination corrections were created by stacking the image frames in each filter, with high and low rejection to remove objects, and then boxcar smoothing the stacked image. The individual fields were registered to a common position in each filter, and then stacked using a weighted average. The weights were determined by measuring the signal to noise for several randomly chosen stars on each frame. The stacked images for each filter were then registered to a common image to simplify the photometric measurement in matched apertures. The final images for each of the three runs were then registered and stacked again using the weighted average.

Object detection and photometry were performed using a custom pipeline. The object detection was done separately in each filter using the SExtractor package (Bertin & Arnouts 1996). The separate detections in each filter were then matched using a growing annulus technique in the order of B , U , R , then I and a master detection list was produced. Using this list, photometry was determined in both SExtractor’s modified Kron (Kron 1980) aperture and a $10''$ diameter aperture matched in each band. The actual photometry algorithm used involved a modification to SExtractor in both the background calculation and pixel assignment within the aperture of interest. The detections were photometrically calibrated using published standards (Landolt 1992) which were measured at similar airmasses to the object frames. The photometric zeropoint was then adjusted to the AB system (Oke & Gunn, 1983) using published transformations (Fukugita *et al.* 1995): $U_{AB} = U + 0.69$, $B_{AB} = B - 0.14$, $R_{AB} = R + 0.17$, and $I_{AB} = I + 0.44$.

Astrometric transformations were determined from the *HST* Guide Star Catalog II (Lasker 1996), after which the redshifts in the Canada France Redshift Survey (CFRS) 14 hour field were matched to our photometric sample. The measured dispersion between the CFRS I_{AB} isophotal magnitudes and our I_{AB} automatic magnitudes was $\sigma \approx 0.13$ to $I \sim 23$ with no evident systematic deviations from a linear relationship.

3. Analysis

In an effort to minimize the dispersion in our relationship, we imposed two conditions on the data used in this analysis. First, we restricted the photometric sample such that all object magnitudes were below the appropriate magnitude limit at which a typical galaxy had a measured $1\sigma_{rms}$ magnitude error of approximately 0.1 magnitudes. Second, we required that only the most reliable spectroscopic identifications be incorporated into the fitting procedure. This involved pruning the CFRS catalog such that only non-stellar objects with redshifts having a confidence greater than 95% were retained. This was accomplished by restricting the redshifts used to the following quality classes: 3,4,8,93,94,98 (*cf.* Le Fevre *et al.* 1995).

The final sample contained 89 redshifts with the following distribution: 40 redshifts in the range (0.0, 0.4] and 49 redshifts in the range (0.4, 0.8]. For these two subsets, we fit a second order polynomial in $U B R I$, $U B R$, and $B R I$ to the measured photometry and published redshifts. In each region, the degrees of freedom remained a substantial fraction of the original data (a second order fit in four variables requires 15 parameters). This technique is a simple approach designed to quantify the accuracy of our method for estimating redshifts and is not the optimal parameterization of the topology of the galaxy distribution, which is the subject of ongoing work.

EDITOR: PLACE TABLE 1 HERE.

The redshift intervals were not chosen randomly. This technique has been previously shown to be more sensitive to broad spectroscopic continuum features (primarily the break in the continuum spectra at around 4000 \AA , which moves between the B and R bands at $z \approx 0.4$, and the R and I bands at $z \approx 0.8$) rather than specific absorption/emission features (Connolly *et al.* 1995). This is clearly demonstrated in Table 1 where the standard deviation in the redshift range $(0.0, 0.4]$ is only slightly higher when the I band is not included in the fit. On the other hand, when the U band is excluded from the fit, the standard deviation more than doubles. This reflects the fact that the I band is sampling the same flat region of the spectrum as the R band within this redshift range, and is thereby providing predominantly redundant information to the fit. In the second redshift range, the continuum break is moving from the B band into the R band, which is reflected in the lower significance of the U band information. We also show the expected intrinsic dispersion in this relationship from simulations using all four bands (*cf.* Connolly *et al.* 1995), which clearly shows that our measured dispersion is completely dominated by the intrinsic scatter within the relationship.

EDITOR: PLACE FIGURE 1 HERE.

The relative importance of the different bands in the individual redshift intervals reflects the curvature inherent within the distribution of galaxies in the multi-dimensional magnitude space. In a given redshift range, the curvature is accurately parameterized by a second order polynomial. Between redshift intervals, however, the distribution displays a higher order curvature term (*cf.* the previous discussion concerning the continuum break), which requires the use of a piecewise second-order parameterization. As a result, the application of these results requires an iterative approach. First, a third order global

photometric redshift relation is used to determine an approximate redshift. From this initial redshift estimate, the appropriate second-order relationship can then be used. If the initial estimate is on the border between two subsets ($z \in [0.35, 0.45]$), both relationships should be applied and the mean of the two results used.

With the introduction of the four-vector $C = (U, B, R, I)$, the second-order photometric-redshift relationships can be summarized in the following manner:

$$z = Z_\alpha + C \cdot V_\alpha + C \cdot M_\alpha \cdot C^T$$

where the scalar Z_α , vector V_α , and matrix M_α components are listed in Table 2 for the two different redshift regimes. The parameters for the third order fit are listed in Table 3.

4. Discussion

We have shown that using a simple iterative process, redshifts can be reliably estimated for objects from broadband photometry out to $z \sim 0.8$. A comparison of our measured dispersion with the published intrinsic dispersion from simulations (Connolly *et al.* 1995) indicates that we have approached the inherent scatter within the photometric-redshift relationship. These simulations provide an absolute lower limit to the intrinsic scatter, as they only assumed an evolved (15 Gigayear) SED. As the additional effects of metallicity, dust, and stellar histories can only increase the scatter within the relationship, we do not include them in our estimation of the minimal intrinsic scatter within the photometric-redshift relation.

Thus it is quite remarkable that we measure such a small scatter as compared to the simple, single age, solar metallicity, and dust free galaxies produced in the simulations. Actual galaxies are clearly more complex, spanning a wide range of star formation histories, ages, metallicities, and dust content, all of which would be expected to significantly increase

the measured dispersion. We see that this is not the case, which leads us to two related conclusions. First, this technique is extremely dependent on the 4000 Å break which is present in nearly all galaxies. Second, metallicity, dust, and age variations have similar effects in this multidimensional space, albeit almost orthogonal to the redshift vector (Koo 1986). We plan on improving our understanding of the multidimensional nature of the observed galaxy population through the use of SED modeling. This will allow us to quantify the importance of the metallicity, dust, and different stellar histories and explore any possible degeneracies.

The photometric-redshift estimation technique can be considered to be the equivalent of a low resolution (4 element) spectrograph. By using more filters that are increasingly narrow, we increase the spectral resolution of this technique. Taken to the extreme, however, this approach will emulate a spectrograph, losing the observing efficiency that is the primary advantage of this technique. From a comparison between the dispersion from the three band and the four band quadratic fits, it is clear that a marginal gain is achieved by adding a fourth band within a given redshift regime. As a result, we believe that the benefits achieved by adding more bands to this approach is more than offset in the loss of observational efficiency. The simulations used the standard U , B , R , & I filters in order to be reliably compared to our observations.

We are working to extend this analysis in two principal areas. First, we are now focusing on improving our understanding of the distribution of galaxies in this multi-dimensional flux space. This requires the use of a stratified sampling strategy to obtain redshifts throughout the photometric sample. These additional redshifts are primarily being obtained using the Keck telescope within the DEEP collaboration. In addition, we are incorporating additional physical parameters (*eg.* surface brightness and shape parameters) via *HST* WFPC2 imaging to quantify the different morphological tracts within the cumulative

galaxy distribution.

Second, we are extending this work to higher redshifts. For redshifts below $z \sim 1.2$, we are working to increase the size and stratification of our redshift sample. This involves increasing our photometry-redshift catalog through the addition of published redshifts and our participation in several spectroscopic surveys. In the redshift region $1.2 \leq z \leq 2.8$, we are adding near-infrared photometry to our catalog in order to sample the continuum features our technique requires. Until a large quantity of reliable spectra can be obtained within this region (the arrival of the blue camera on LRIS will help alleviate this quandary), we will use our understanding of the $z < 1.2$ regime and the published high z work of others (Steidel *et al.* 1996) as boundary conditions. We can then use SED models to extrapolate into this region, while maintaining the boundary condition requirements at both redshift ends. As spectra in this area become available, we will add them into the fitting procedure. Eventually this work will allow for the estimation of not only the redshift, but also the spectral type of an object solely from broadband photometry.

First we wish to acknowledge Gyula Szokoly for assistance in obtaining the data. We also would like to thank the referee for useful comments, and Barry Lasker, Gretchen Greene, and Brian McLean for allowing us access to an early version of the GSC II. We also wish to acknowledge useful discussions with Mark Dickinson, Mark Subbarao, and David Koo. RJB would like to acknowledge support from the National Aeronautics and Space Administration Graduate Student Researchers Program. AJC acknowledges partial support from NASA grant AR-06394.01-95A. ASZ has been supported by the NASA LTSA program.

REFERENCES

- Baum, W.A. 1962, Problems of Extragalactic Research, IAU Symposium No. 15., 390.
- Bertin, E., & Arnout, S., 1996, A&AS, 117, 393.
- Brunner, R.J, PhD. Thesis, The Johns Hopkins University, 1997.
- Connolly, A.J., Csabai, I., Szalay, A.S., Koo, D.C., Kron, R.G., and Munn, J.A., 1995, AJ, 110, 6.
- Fukugita, M., Shimasaku, K., Ichikawa, T., 1995, PASP, 107, 945.
- Koo, D.C., 1985, AJ, 90, 418.
- Koo, D.C., 1986, ApJ, 311, 651.
- Kron, R.G., 1980, ApJS, 43, 305.
- Landolt, A.U. 1992, AJ, 104, 340.
- Lasker, B., 1996, Private Communication.
- Le Fevre, O., Crampton, D., Lilly, S.J., Hammer, F., and Tresse, L., 1995, ApJ, 455, 60.
- Loh, E.D., & Spillar, E.J., 1986, ApJ, 303, 154.
- Oke, J.B., & Gunn, J.E., 1983, ApJ, 266, 713.
- Steidel, C.C., Giavalisco, M., Pettini, M., Dickinson, M., & Adelberger, K.L., 1996, ApJ, 462, L17.

Table 1. The standard deviation between measured and estimated redshifts.

Redshift Range	$\sigma_Z(UBRI)$	$\sigma_Z(UBR)$	$\sigma_Z(BRI)$	$\sigma_Z(Simulation)$
(0.0,0.4]	0.0234	0.0301	0.0498	0.016
(0.4,0.8]	0.0389	0.0834	0.0431	0.043

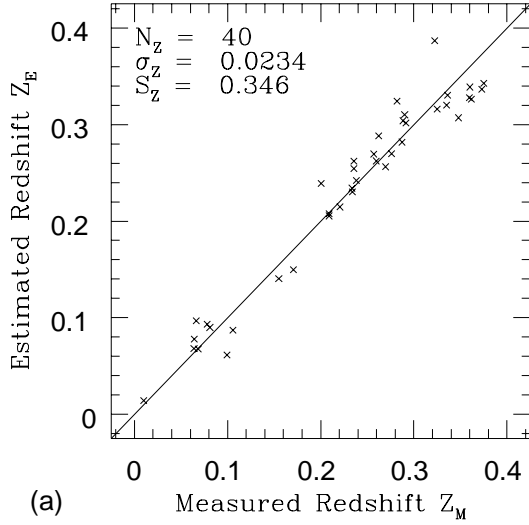
Table 2. The 2^{nd} order polynomial terms.

Redshift Range	Scalar	Vector	Matrix				
			U	B	R	I	
(0.0,0.4]	0.987	-1.239	0.1168	-0.25660	-0.17239	0.23456	U
		1.513	0.0	0.16295	0.12049	-0.23008	B
		2.099	0.0	0.0	-0.22036	0.39080	R
		-2.476	0.0	0.0	0.0	-0.14324	I
(0.4,0.8]	7.31	0.7245	0.32111	-1.1314	0.83587	-0.36212	U
		-2.493	0.0	0.97325	-1.3183	0.58085	B
		5.378	0.0	0.0	0.52568	-0.78022	R
		-4.225	0.0	0.0	0.0	0.36975	I

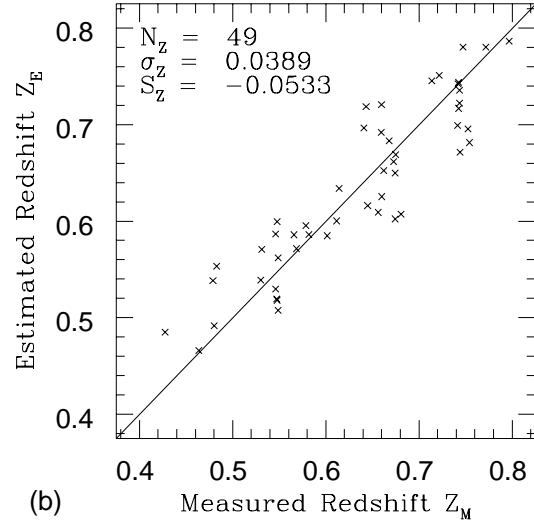
Table 3. The 3rd order polynomial terms.

Scalar	Vector	Matrix				
		U	B	R	I	
-31.5	-3.209	11.933	-26.217	-33.532	35.985	U
	-18.34	0.0	17.690	38.390	-46.131	B
	117.7	0.0	0.0	-32.404	50.319	R
	-90.97	0.0	0.0	0.0	-16.296	I
Third Order Terms		U	B	R	I	
26.391	UBR	-1.5113	7.9136	-8.0678	4.1007	U ²
-12.859	UBI	-13.988	8.4890	-23.815	11.322	B ²
-2.1809	URI	-3.3766	13.023	-5.5753	8.2411	R ²
-6.0829	BRI	2.6542	-0.91194	-5.1008	1.3397	I ²

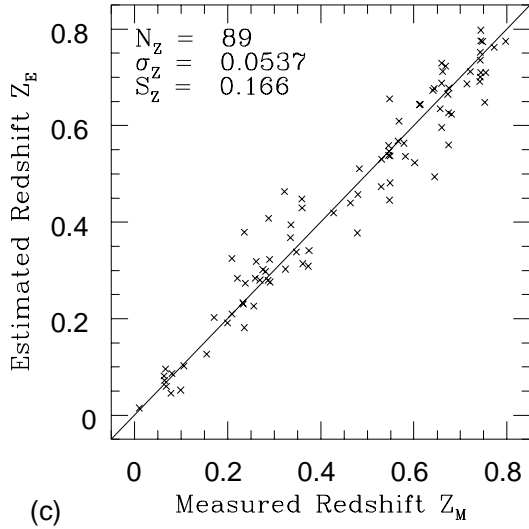
Fig. 1.— The correlation between estimated and measured redshifts are shown in (a) for the second order fit in the redshift interval $(0.0,0.4]$, (b) for the second order fit in the redshift interval $(0.4,0.8]$, and (c) for the third order fit in the redshift interval $(0.0,0.8]$. Indicated in each figure are the number of redshifts (N_Z), dispersion (σ_Z), skewness (S_Z), and a straight line of unit slope, which is not a fit to the data. A histogram of the residuals for the third order fit are displayed in (d).



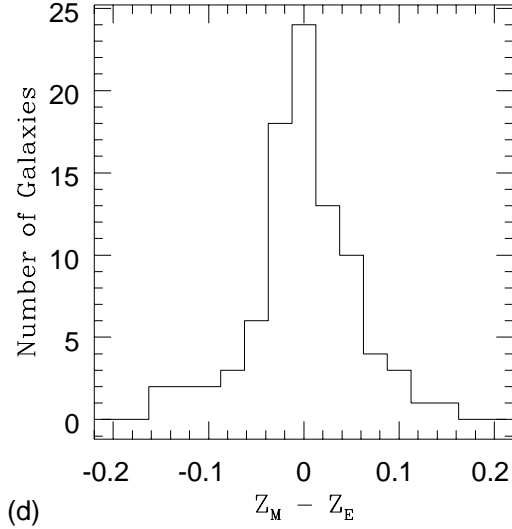
(a)



(b)



(c)



(d)